Earth Surf. Dynam. Discuss., https://doi.org/10.5194/esurf-2018-47
Manuscript under review for journal Earth Surf. Dynam.
Discussion started: 22 June 2018
© Author(s) 2018. CC BY 4.0 License.

Measuring Subaqueous Progradation of the Wax Lake Delta with a Model of Flow Direction Divergence

John B. Shaw[1], Justin D. Estep[1,2], Amanda R. Whaling[1], Kelly M. Sanks[1], Douglas A. Edmonds[3]

[1]Department of Geosciences, University of Arkansas, Fayetteville, 72701, USA
[2]Department of Geology and Geophysics, Texas A&M University, College Station, 77843, USA
[3]Department of Earth and Atmospheric Sciences, Indiana University, Bloomington, 47405, USA

Correspondence to: John B. Shaw (shaw84@uark.edu)

Abstract. Remotely sensed flow patterns can reveal the location of the subaqueous distal tip of a distributary channel on a prograding river delta. Morphodynamic feedbacks produce distributary channel tips that become shallower over their final reaches before becoming deeper over the unchannelized foreset. The flow direction field over this morphology tends to diverge and then converge providing a diagnostic signature that can be captured in flow or remote sensing data. Twenty-one measurements from the Wax Lake Delta (WLD) in coastal Louisiana, and 317 measurements from numerically simulated deltas show that the transition from divergence to convergence occurs in a distribution that is centered just downstream of the channel tip, on average 132 m in the case of the WLD. With these data we validate the Flow Direction to Channel tips (FD2C) inverse model for remotely estimating subaqueous channel tip location. We apply this model to 33 remotely sensed images of the WLD between its initiation in 1974 and 2016. We find that the distributaries grew unevenly, 6 of the primary channels grew at rates of 60-80 m/yr while one grew at 116 m/yr. We also estimate the growth rate of the total area enclosed by the subaqueous delta platform to be 1.83 km^2/yr with no obvious rate changes over time.

1 Introduction

River deltas host productive ecosystems and hundreds of millions of people worldwide. Over the past century, river deltas have changed rapidly, putting these large human populations at risk (Barras et al., 2008; Erban et al., 2014; Wilson et al., 2017; Wu et al., 2017). Monitoring morphologic change on river deltas is key to their sustainable management (Peyronnin et al., 2017). Remote sensing techniques provide synoptic monitoring of deltas, but are generally limited to monitoring subaerial or very shallow regions (Couvillion et al., 2011; Li and Damen, 2010; Rahman et al., 2011; Rangoonwala et al., 2016). However, most deltas are far larger than their sub-aerial portions. For instance, the subaerial area of the Wax Lake Delta in 2015 was 50 km^2 (Olliver and Edmonds, 2017) while the subaqueous area was an additional 82 km^2 (Shaw et al., 2016a). The difference arises because the Wax Lake Delta has an extensive delta front deposit that lies below low tide. While the subaerial and shallow land area are where marshes are established (Johnson et al., 1985), the subaqueous delta forms the platform upon which subaerial islands grow (Cahoon et al., 2011; Shaw et al., 2018). Hence, the subaqueous platform extent is important as a leading indicator of future marsh growth, necessary data for navigation, and the key area metric for estimating delta volume and volume

Earth Surf. Dynam. Discuss., https://doi.org/10.5194/esurf-2018-47
Manuscript under review for journal Earth Surf. Dynam.
Discussion started: 22 June 2018
© Author(s) 2018. CC BY 4.0 License.
Earth Surface Dynamics Discussions

change (Geleynse et al., 2015). Unfortunately, only a small fraction of global river deltas have been directly surveyed in a manner to resolve changes to the subaqueous portion of deltas. This is partly due to the vast area of deltas, and partly because year-round turbidity fundamentally limits bathymetric lidar or multispectral remote sensing techniques (Gao, 2009). Many shallow regions along the US coast far from navigation corridors have not been officially surveyed since the 1930s (e.g. NOAA, 2017).

Here we make progress in subaqueous delta monitoring techniques by recognizing key connections between delta front bathymetry and the flow field that organizes over it. We then exploit this connection by remotely sensing the flow direction using streaklines on the water surface visible on some deltas (Figure 1). We use the Wax Lake Delta as a field site due to available bathymetric maps and because it frequently exhibits streaklines that resolve delta front flow directions. In section 2, we review the coupling of emergent delta front bathymetry and flow patterns. In section 3, we present the flow direction to channel (FD2C) model of estimating the location of channel tips using the remotely sensed flow direction field. In section 4, the model is validated on the Wax Lake Delta and with four numerical models of deltas. The model is applied to 33 images of the Wax Lake Delta spanning its development from 1974 to 2016 in section 5 in order to estimate progradation rates of individual channels as well as growth rate of total delta area. The strengths and limitations of the model and results from its application are discussed in section 6.

2 Bathymetry and Flow Patterns on River-Dominated Deltas

There is virtually no limit to the paths that a parcel of water can trace across a domain with arbitrary bathymetry and boundary conditions. The seemingly unlimited degree of freedom limits the skill of inverse models that place no constraints on the possible bathymetry (Alpers et al., 2004; Romeiser and Alpers, 1997). However, direct study of river deltas reveals that emergent patterns can be found with their bathymetry and flow patterns. If the bathymetry and flow take on predictable patterns, this greatly reduces the degrees of freedom in a system, improving predictability. The postulation of emergent flow patterns has a long tradition in coastal geomorphology (e.g. Edmonds and Slingerland, 2007; Wright, 1977). Extensive work has been done to predict initial flow and sedimentation patterns associated with turbulent jets entering basins (Fagherazzi et al., 2015). Our work seeks to extend this approach to systems with complex emergent topography and multiple interacting channels. If a certain bed morphology produces distinct flow patterns visible on remotely sensed imagery, then that pattern can be used to predict the underlying morphology. We make this case for the flow patterns on the delta front on a prograding delta.

For well-developed, prograding river deltas, the bed morphology of a channel terminus can be idealized as an adverse bed slope (shallowing with distance downstream) along the thalweg and basinward levee slopes (deepening with distance), which together produce a gradual loss of channel confinement (Figure 2). Channels lose definition at the channel tip where the thalweg elevation equals the levee elevation. This transition occurs gradually; over >7 channel widths for the Wax Lake Delta. (Shaw and Mohrig, 2014). Beyond the location where channel definition is lost, the unchannelized bed slopes basinward over

© Author(s) 2018. CC BY 4.0 License.

the delta foreset. Importantly, the point where the channel loses definition is also near the maximum elevation in an axial transect of the channel. Although dimensions vary, this general morphology has been observed on the Wax Lake Delta (Shaw et al., 2016b; Shaw and Mohrig, 2014), Brant's Pass crevasse on the birds-foot delta of the Mississippi River (Esposito et al., 2013), the Mobile and Apalachicola river deltas (Edmonds et al., 2011b) and the St. Clair River Delta (Figure 1b; NOAA, 2017). Additionally, numerical models often produce this morphology (Caldwell and Edmonds, 2014; Geleynse et al., 2010; Liang et al., 2016). These deltas can be qualitatively classified as river-dominated (Galloway, 1975), both by their large fluvial sources and relatively small winds and tides. Strong waves and tides can significantly alter this morphology (Leonardi et al., 2013; Nardin and Fagherazzi, 2012). Hence, we limit ourselves to river-dominated conditions here. Recently, flow patterns have been measured across channel tips on the Wax Lake Delta. Various techniques have been used to show that on Gadwall Pass on the Wax Lake Delta (Figure 1a, 3), roughly 50% of water discharge leaves channels laterally (Hiatt and Passalacqua, 2015; Shaw et al., 2016b). This is due to hydrological connectivity between the distributary channels and interdistributary bays over subaqueous levees, and due to reduction of channel cross-sectional area over this reach (Coffey and Shaw, 2017; Hiatt and Passalacqua, 2017). One way to track the flow field in this transitional zone is through streaklines on the water surface. In many coastal settings, slicks of naturally occurring oil and biogenic debris accumulate on the air-water interface (Alpers and Espedal, 2004; Espedal et al., 1996; Garabetian et al., 1993). Despite thicknesses on the order of nanometers, streaks produced by this material are readily observed from boats (Espedal et al., 1996), in near-infrared aerial and satellite imagery as well as from synthetic aperture radar backscatter (Hühnerfuss et al., 1994). Shaw et al. (2016b) showed that such streaklines track direct measurements of the depth-averaged flow direction across the delta front of the Wax Lake Delta with reasonable accuracy, even when the ground-truth and remote sensing measurements were made months apart. Similar streakline patterns have been observed on other delta fronts as well (Figure 1). Our cursory analysis suggests that streaklines form mostly on deltas with established marshes that flow into freshwater basins or river discharge is enough to make the proximal receiving basin fresh. The latter condition characterizes the Wax Lake Delta and Atchafalaya Bay (Holm and Sasser, 2001; Li et al., 2011).

While streaklines record the depth-averaged flow direction field, they provide no information about the flow velocity magnitude (speed). However, if $\vec{\boldsymbol{d}}$ is the unit vector field aligned with the local flow direction (dimensionless), h is the flow depth field (L), $|\vec{U}|$ is the velocity magnitude field (L/T), and temporal variations (*dh/dt*) are minimal, then conservation of fluid mass can be manipulated to produce a set of equations that relate acceleration ($\breve{A}$), vertical constriction ($\breve{B}$), and lateral divergence ($\breve{D}$; Shaw et al., 2016b):

$$\breve{A} = \breve{B} + \breve{D} \tag{1a}$$

$$\breve{A} = \frac{\nabla|\vec{U}| \cdot \vec{\boldsymbol{d}}}{|\vec{U}|} \tag{1b}$$

$$\breve{B} = -\frac{\nabla h \cdot \vec{\boldsymbol{d}}}{h} \tag{1c}$$

© Author(s) 2018. CC BY 4.0 License.

$$\breve{D} = -\nabla \cdot \vec{\boldsymbol{d}} \tag{1d}$$

Analysing flow patterns on the delta front downstream of Gadwall Pass on the Wax Lake Delta, Shaw et al. (2016b) found that adverse bed slopes ($\breve{B} > 0\ \mathrm{m}^{-1}$) were generally associated with flow direction divergence ($\breve{D} < 0\ \mathrm{m}^{-1}$). In contrast, downstream of the channel tip on the basinward sloping delta foreset $\left(\breve{B} < 0\ \mathrm{m}^{-1}\right)$ the flow direction field converged $\left(\breve{D} > 0\ \mathrm{m}^{-1}\right)$. The transition from negative to positive $\breve{D}$ occurred just 400 m (two channel widths) away from the channel tips.

Converging flow direction field for delta front flows are counter-intuitive: turbulent jets emanating from channel mouths generally expand ($\breve{D} < 0\ \mathrm{m}^{-1}$) with distance downstream (Kundu et al., 2011) due to lateral shear with still water or bed friction. However, scaling of shallow water jets by Özsoy and Ünlüata (1982) showed that in the presence of significant basinward slopes, jets can converge or contract when the basinward bed slope ($-\nabla\eta \cdot \vec{\boldsymbol{d}} \approx \nabla h \cdot \vec{\boldsymbol{d}} > 0$) exceeds the dimensionless friction factor (C_f). Recent numerical modelling by Jiménez-Robles et al. (2016) also shows that jets can exhibit flow direction convergence when basinward slopes exceed ~1%. The bathymetric complexity and significant unchannelized flows on the Wax Lake Delta prevent us from rigorously applying the findings of either study to the delta front of the Wax Lake Delta, but note that there is a physical basis for flow direction convergence on delta fronts that supports the convergence we observe in streaklines.

3 The FD2C Model

If a channel tip's location controls the flow direction field, we seek an inverse method of estimating the channel tip location from the flow direction field that can be used with remotely sensed imagery. Previous analysis (see Section 2) showed that the transition from adverse bed slopes to basinward bed slopes at channel tips is coupled with the transition from flow divergence to flow convergence as tracked by streaklines. We name this model of coupled bathymetry and flow the C2FD model ("Channel to Flow Divergence"), where channel tips control the flow direction field. If this correlation is persistent and predictable, then the location of the channel tips can be related to a critical point in the $\breve{D}$ field ($x_{\breve{D}}$). Analysis of the Wax Lake Delta and numerical delta simulations show that $x_{\breve{D}}$ is where $\breve{D} = 0\ \mathrm{m}^{-1}$ and $\breve{D}$ is changing from negative to positive in the downstream direction (Figure 2). We name this inverse model FD2C for "Flow Divergence to Channel tips."

3.1 Application

The $\breve{D}$ field can be calculated using streaklines (Figures 3, 4). First, we trace the curvilinear shape of all streaklines manually in ArcGIS. Streaklines are also mapped down the center of primary distributary channels, although streaklines rarely occur there. This is done because flow direction is generally found to follow the trends of large channels. Assuming that the local flow direction is everywhere tangent to the streakline, we sample each streakline at 25 m increments along the line, noting the

© Author(s) 2018. CC BY 4.0 License.

local direction of the line. This produces a dataset of points $P(x, y, \vec{\boldsymbol{d}})$, where x and y are the Easting and Northing spatial coordinates (UTM Zone 15N) and $\vec{\boldsymbol{d}}$ is the unit vector tangent to the mapped streakline. Flow direction $\vec{\boldsymbol{d}}$ is recorded as a unit vector with components in the x and y directions: $\vec{\boldsymbol{d}} = (d_x, d_y)$, $(d_x^2 + d_y^2 = 1)$. The flow direction field is then constructed by interpolating d_x and d_y independently from P. We use the biharmonic spline interpolation technique of Sandwell (1987) because of the smooth interpolation results. The resulting fields were again normalized by their magnitude $|\vec{\boldsymbol{d}}| = d_x^2 + d_y^2$ to insure the field remained unit vectors. Finally, the flow convergence field $\breve{D}$ is calculated on the grid as $\breve{D} = -\nabla \cdot \vec{d} = -\left(\frac{\partial d_x}{\partial x} + \frac{\partial d_y}{\partial y}\right)$ (Figure 3b). On numerical models (Figure 4), the $\breve{D}$ field was calculated directly from the modeled depth averaged velocity field and thus required no interpretation of streaklines or field interpolation, so the $\breve{D}$ field is exact in that case.

3.2 Estimating Channel Tip Location

We test the FD2C model by comparing the location of channel tips to the critical divergence point $\breve{D}_{cr}$ on the Wax Lake Delta and numerical model, as well as on a set of numerically modelled deltas. For each primary distributary channel, we draw transect down the center of the subaerial reach of the distributary channel extending into the basin (Figure 4) and track bathymetry ($\eta(x)$) and flow direction divergence ($\breve{D}(x)$) as a function distance x along it (Figure 5). The channel tip, $\hat{\eta}$ is defined as the global maximum elevation along the transect and the location defined as $x_{\hat{\eta}}$. The critical divergence point ($x_{\breve{D}}$) is defined as the first downstream location where both $\breve{D} = 0\ \mathrm{m}^{-1}$ and $d\breve{D}(x)/dx > 0\ \mathrm{m}^{-2}$. The difference $\Delta l = x_{\breve{D}} - x_{\hat{\eta}}$ is defined as the distance downstream of the channel tip where the critical divergence point occurs (Figure 5). Note that if $\Delta l < 0$ m, then the critical divergence point occurs upstream of the channel tip.

3.3 Validation

Summary statistics of Δl (Table 1, Figure 6) provide a means of testing the FD2C model, which states that Δl is generally small. Data was drawn from the Wax Lake Delta by comparing delta front bathymetry collected in July 2010 (2 channel tips), August 2011 (6 tips), February 2015 (6 tips), and July 2016 (7 tips) to imagery from 14 October 2010, 1 October 2011, 19 April 2015, and 5 April 2016 respectively. Over these 21 measurements, Δl had a mean of 145 m and a median of 132 m (Figure 6a). The sample had an interquartile range of 701 m (Table 1, Figure 6). This supports the claim that $\breve{D}_{cr}$ is generally near $\hat{\eta}$. While the variation of Δl is significant, it constitutes just a 7% uncertainty for a delta that is presently about 10 km long.

In order to achieve some validation independent of the Wax Lake Delta, the FD2C model was also evaluated on four numerical river deltas originally presented by Caldwell and Edmonds (2014). These deltas were modelled using Delft3D on a 25 x 25 m^2 grid. Model runs A1a1, A1e1, D1a1, and D1e1 were used. These runs had an upstream discharge of 1000 m^3/s and no tidal or

© Author(s) 2018. CC BY 4.0 License.

wave forcing. They differed in incoming median grain diameter between 0.01 and 0.1 mm, the sorting of the sediment distribution, and the fraction of the sediment that was cohesive. Full descriptions of the runs are found in Caldwell and Edmonds (2014). Measurements began at time step 500 to allow a significant deposit to develop and then every 5 time steps thereafter. At each time step, up to 5 of the largest distributary channels in terms of flow velocity were measured. Fewer measurements were made if less than 5 channels were present. These analyses yielded a total of 374 samples (Table 1).

For the four modelled deltas, the median Δl ranged from 12 m to 199 m (Figure 6a). While the ranges of Δl were up to 2110 m in the case of D1e1, the interquartile ranges were between 156 to 254 m. Some transects drawn on numerical deltas did not yield $x_{\breve{D}}$ because the criteria for $x_{\breve{D}}$ were not met. This meant that Δl could not be measured and the FD2C method could not be applied. Such cases accounted for 17% of the transects on delta A1a1 and 21% of delta D1a1 (Table 2) and 8% of the total transects measured on numerical deltas.

Measurements from the modelled deltas also show the distribution of Δl is relatively stable over time (Fig. 6b). A linear regression was fit to Δl versus time and the slope of the data was not significant by a *t*-test ($p > 0.10$ for each numerical delta). Therefore the null-hypothesis that there was no trend in the data cannot be rejected. This stationarity suggests that Δl does not change, even as a delta progrades. We also investigated whether Δl is a function of upstream channel width and flow depth at the channel tip (Supplementary Material). However, none of these parameters showed predictive power over Δl.

Taken together, these data validate the FD2C method for prograding deltas with several distributary channels. Measurements from the Wax Lake Delta and numerical models all show that the central tendency is for Δl to be about 100 m, and model data shows that the distribution remain stationary over time and delta growth. We apply this result to the Wax Lake Delta to measure the growth of its subaqueous channel tips.

4 Tracking Wax Lake Delta progradation with the FD2C model

4.1 Methods

The FD2C method was applied to estimate the locations of channel tips over time on the Wax Lake Delta using 33 images between 30 January 1974 and 5 April 2016. Images are near infrared imagery from Landsat 2, 5, and 8, SPOT and an overhead photomosaic. See Supplementary Material for details regarding the imagery. For each image, the FD2C method (Section 3) was applied by mapping a transect starting at the edge of subaerial exposure (delta shoreline) and extending along the 7 primary distributary channel axes of the WLD (Figure 3b) to find $x_{\breve{D}}$. The first two images (30 January 1974 and 9 February 1979) showed minimal subaerial delta exposure, so transects were mapped over abrupt changes in $\breve{D}$ and grouped to East Pass in the eastern portion of the delta, Gadwall Pass in the central portion of the delta, and Campground Pass in the western portion of the delta. The channel tip location was then estimated as $x_{\breve{D}} - \Delta l$, or an average 145 m upstream of $x_{\breve{D}}$ according to

© Author(s) 2018. CC BY 4.0 License.

measurements from the Wax Lake Delta itself (Figure 6, Table 1). Channel tip growth was then tracked as the Euclidian distance between the delta apex (UTM Zone 15N: 651673 E 3267186 N).

Estimated channel tips were connected to one another and the pre-delta shoreline to measure the area within the delta's subaqueous platform. Each channel tip occurs at a crest in bathymetric elevation and progrades via erosion of the deposit in front of it. By connecting these tips, we enclose an area that has received significant deposition, but not yet enough to become subaerially emergent, even at low tide. The enclosed area also contains channels and all subaerially emergent regions, but excludes some sea-ward deposition associated with the delta forest. We name the region the total delta area. Monte Carlo techniques were used to include uncertainty in Δl in calculating the platform area. First, $x_{\tilde{D}}$ was found for each of the seven primary distributary channels using the technique above. The location of $x_{\hat{\eta}}$ was determined by randomly sampling a measured value of Δl for the Wax Lake Delta (Figure 5a), and then estimating the location of the channel tip $\left(x_{\hat{\eta}} = x_{\tilde{D}} - \Delta l\right)$. The seven channel tips were then connected by straight lines, and then connected to a pre-delta shoreline of Atchafalaya Bay mapped from 1974 imagery (Figure 3). The pre-delta shoreline extends 10 km up the original Wax Lake estuary (Shlemon, 1972), however delta area is truncated north of 3269274 N in order for area results to be more comparable to existing datasets. The truncated area of the original Wax Lake estuary is 17.2 km^2, and can be added to all area estimates if desired. In order to join the straight lines connecting channel tips to the pre-delta shoreline, the East Pass channel tip was connected to the pre-delta shoreline with a ray with a 27° azimuth (Figure 3b). The Campground Pass channel tip was connected to the mainland with a ray of 0° azimuth. These azimuths were chosen to accurately reflect the marginal deposition on the Wax Lake Delta over the imagery used in the study. Total area is not sensitive to these choices. The area of the resulting polygon was calculated 10^4 times with different random sampling to account for the distribution of Δl (Monte Carlo sampling). The 16th, 50th, and 84th percentile of areas were then recorded for a given image. This process was repeated for each image to track delta area over time.

4.2 Results

Channel tip progradation rates are shown in Fig. 7. Between 1974 and 2016, each of the seven primary distributary channels extended at least 2 km. In clockwise order, East, Pintail, Greg, Main, Gadwall, Mallard, and Campground Passes had average progradation rates of 74 ± 9 m/yr, 75 ± 13 m/yr, 89 ± 13 m/yr, 73 ± 10 m/yr, 116 ± 10 m/yr, 66 ± 15 m/yr, 60 ± 20 m/yr. All primary distributary channels, except Gadwall Pass, grew at similar rates between 60 ± 20 (Campground) and 89 ± 13 m/yr. In contrast, Gadwall Pass grew at a significantly faster rate of 116 ± 10 m/yr. Looking beyond simple linear regression, we checked for secular changes in channel tip growth rate over time using the "segmented" package in R (Muggeo, 2003). However, no significant breakpoints in growth rate were found.

The delta area estimated using the FD2C method is shown in Fig. 8. The delta area shows an apparently linear increase in area over time from 38.6 km^2 in 1974 to 113.4 km^2 in March 2016. The growth rate over this period is 1.71 ± 0.13 km^2/yr. The data

© Author(s) 2018. CC BY 4.0 License.

points have a root-mean-square error of 7.86 km^2 compared to the linear regression. This uncertainty generally falls within the standard error for the estimation of the area at a given time, which averages 13.69 km^2 over the length of the dataset.

5 Discussion

5.1 The FD2C Model

The FD2C conceptual model assumes that water leaving a self-formed distributary channel will have a flow direction field that first diverges $(\breve{D} < 0)$ and then converges $(\breve{D} > 0)$ with the transition between the two fields occurring near the channel tip where the bathymetric elevation peaks and the channel loses definition. This model was supported by measurements from Wax Lake Delta and four Delft3D model runs (Figures 5, 6). Analysis of Δl using modelled deltas also confirms that there is no significant trend in Δl with time. We use this to assume that the distribution of Δl is stationary and the modern distribution can be applied to the delta in the past. This is important, because field measurements on the Wax Lake Delta from the past 5 years do not provide the time-resolution to confirm this independently.

Each of the Δl distributions have significant standard deviations (Table 1). This suggests that although the FD2C conceptual model is accurate to first order, other processes also affect Δl. We discuss a few possibilities here. First, the variation could stem from channel properties. If two channels are near one another, their outflows and the unchannelized flow between them would be constricted compared to a channel that is far from its neighbours. This may be particularly important in places like the Eastern portion of the Wax Lake Delta, where Main, Greg, Pintail, and East passes enter Atchafalaya Bay over about 8 km (Figure 3a). Second, the variation in Δl could stem from non-steady forcing. Temporal variations in flow such as tides or wind set-up of the water surface likely affect the flow direction field to some degree. For example, once flow departs the delta front, it is clear that during rising tide, the general flow direction mapped by streaklines in the bay is to the northwest into Cote Blanche Bay. During falling tide, flow direction is southward toward the Gulf of Mexico. However, it is less clear how the divergence field is affected, particularly in the shallow delta front where $\breve{D}$ is highly variable. Understanding the connections between these process and flow patterns may significantly influence uncertainty of interpreting channel tip location. However, we note that the Delft3D models had steady boundary conditions (no winds or tides) and still produced a significant distribution, so winds and tides are unlikely to be the chief cause of variability in Δl.

The Δl distributions of the Delft3D deltas were tighter than the distribution for the Wax Lake Delta (Figure 6, Table 2), with standard deviations that were less than half as large (Table 2). We present two possible explanations for this. First, $\breve{D}$ and bathymetry were calculated directly from model outputs for the Delft3D runs, and therefore were exact. In the Wax Lake Delta case, resolving both $\breve{D}$ and bathymetry required interpolation and assuming that streaklines were flowlines. Although streaklines are good indicators of flow direction (Shaw et al., 2016b), they are not explicitly correct. This leads to variation in $\breve{D}$ that is difficult to quantify from the results presented here.

© Author(s) 2018. CC BY 4.0 License.

The variation of Δl prevents confident interpretations of changes in channel tip location on seasonal or annual timescales. For example, extension and back-stepping of channel tip location on the order of several hundred meters were directly measured on Gadwall Pass between July 2010 and February 2012 (Shaw and Mohrig, 2014). The 512 m standard deviation of Δl prevent these changes from being estimated with confidence. However, certainty in measuring change increases with time. The ~60-116 m/yr growth rates observed on distributary channels grow larger than the standard deviation after 4-9 years. For platform area growth analysis, the standard deviation produced by Monte-Carlo sampling from the Δl distribution is about 8.2 km^2, and progradation rates are calculated to be 1.83 km^2/yr. Hence, for estimating changes in Wax Lake Delta total area, we expect the method to be able to perform on timescales of greater than 4-5 years. More detailed sensitivity may be gained by further study of he controls on Δl.

The FD2C model was validated on the Wax Lake Delta and four numerical models. Each of these deltas were prograding with several active channels where lateral channel migration was minimal. We consider this to be strong evidence that the model is transferrable among similar delta settings. This has considerable applications for extending both spatial and temporal monitoring. There are many modern deltas with delta fronts that are either too vast or too remote to be effectively monitored with direct measurements (Bendixen et al., 2017; Wilson and Goodbred, 2015). Bathymetric estimation using the FD2C method can be used to predict channel tip location for navigation purposes. The method can also be used with the decades of remote sensing imagery that already exist. Our analysis found that streaklines were difficult to measure in Landsat 1 and Landsat 2 imagery, but possible in some cases. Streaklines have also been observed in imagery flown from planes and in SAR imagery (Shaw et al., 2016a). This means that the FD2C method can be used to monitor the decadal change of deltas, ranging from the Wax Lake Delta presented here to other sites such as the West Bay diversion of the main stem Mississippi River where land building and sediment retention are explicit goals (Allison et al., 2017; Andrus and Bentley, 2007; Kolker et al., 2012).

5.2 Subaqueous growth of the Wax Lake Delta

5.2.1 Channel Tip Progradation

The FD2C method allows the progradation rates of individual subaqueous channel tips on the Wax Lake Delta to be measured, and provides new insight into decadal growth patterns of the Wax Lake Delta from its initiation to present. The hypothesis of radially symmetric growth often applied to the Wax Lake Delta (Kim et al., 2009; Paola et al., 2011) is largely supported: six of the seven channels have prograded at rates between 60 and 80 m/yr. However, the consistently larger progradation rate of Gadwall Pass (116 ± 10 m/yr) also suggests that the delta is becoming more asymmetric over time. Future evolution may correct for the dominance of Gadwall Pass, possibly by a soft avulsion (*sensu* Edmonds et al., 2011a) reducing Gadwall's growth at the price of another channel. However, the consistently dominant growth rates since 1983 (Figure 7) and the fact that Gadwall Pass is presently the widest channel (Figure 1a, 3a) suggests that this dominance will continue and delta asymmetry will continue to grow.

© Author(s) 2018. CC BY 4.0 License.

5.2.2 Delta Area Growth

Previous studies of delta growth have focused on the emergence of sub-aerial land using Landsat imagery. Allen et al. (2012) investigated the area of subaerial land growth over the entire Wax Lake Delta. They determined a growth rate in Landsat imagery as a function of time, water discharge, and tide level. They found that the subaerial delta grew at a rate of 1.0 km^2/yr between 1983 and 2010. They also interpreted a reduction in growth rate in 2002. Olliver and Edmonds (2017) focused on emergence of just the central islands of the WLD, neglecting some marginal areas of the delta included by Allen et al. (2012). Analyses were based on two images per year selected for minimum and maximum biomass, which mitigated the large swings in area shown by Allen et al. (2012). Linear regression of emergent delta area showed a growth rate of 0.84 ± 0.16 km^2/yr. However, the authors interpreted a break in growth rate at about 1999, with a growth rate from 1984-1999 of 1.88 ± 0.42 km^2/yr and a growth rate from 1999-2015 of 0.78 ± 0.44 km^2/yr.

In all cases, the FD2C method produces delta area estimates that are >40 km^2 larger than estimates of sub-aerial land. The FD2C method is designed to track the location of subaqueous channel tips significantly below any water level datum. Furthermore, the FD2C method includes distributary channels and subaerial land as part of the delta area. Therefore, it stands to reason that the area estimates would be far larger than subaerial methods.

Despite the larger absolute area, the FD2C method yielded growth rates that were similar to previous estimates. The total delta area as measured by the FD2C method grew at a rate of 1.83 ± 0.14 km^2/yr from 1974 to 2016. This suggests that there may be a relatively simple relationship between the subaerial and total delta areas of the Wax Lake Delta. Visual comparison of the Olliver and Edmonds data to the FD2C method (Figure 8) suggest either (a) that the sub-aerial area may be smaller than the total delta constant area by about 70 km^2 or (b) that sub-aerial delta may be a quasi-constant fraction (30-40%) for the total delta area. The data presented here do not clearly favour one interpretation over another. In either case, the growth of the sub-aqueous and sub-aerial portions of the Wax Lake Delta appear to be linked remarkably tightly. This may aid in the prediction of subaerial delta emergence which is key for marsh establishment (Bevington et al., 2017; Johnson et al., 1985; Olliver and Edmonds, 2017; Viparelli et al., 2011), and thereby aid large-scale coastal restoration efforts (Peyronnin et al., 2017).

6 Conclusion

The morphodynamic evolution of channel mouths can produce an emergent delta front deposit morphology and a coupled emergent flow pattern. The delta front morphology consists of subaqueous channels that grow shallower in the downstream direction, subaqueous levees that allow water to exit the channel laterally, and a sloping delta foreset. The flow direction field over this morphology diverges in the final reach of the channel, converges on the delta foreset. The transition from divergence to convergence relative to the channel tip (Δl) varies by many hundreds of meters, but is on average a few hundred meters downstream of the channel tip in both field data from the Wax Lake Delta and numerically modelled deltas. This distribution of Δl appears stationary, allowing it to be applied through time. We present the FD2C method to relate the divergence of flow

Earth Surf. Dynam. Discuss., https://doi.org/10.5194/esurf-2018-47
Manuscript under review for journal Earth Surf. Dynam.
Discussion started: 22 June 2018
© Author(s) 2018. CC BY 4.0 License.

direction estimated using remote sensing of streaklines on the water surface to channel tip location with quantitative uncertainty.

The FD2C method provides a means of estimating the progradation of channel tips and total delta area of the Wax Lake Delta from its initiation in 1974 through 2016. The method involves uncertainties associated with flow field characterization and channel tip location estimation. However, the method allows key aspects of the Wax Lake Delta's progradation to be characterized for the first time such as individual subaqueous channel tip progradation rates and the growth of the total delta area. Channel tips grow at rates ranging from 69-116 m/yr. The subaqueous delta grew steadily between 1974 and 2016 at a rate of 1.83 ± 0.14 km^2/yr, with no clear evidence for changes in growth rate over that period. These estimates can further our understanding of the Wax Lake Delta, which is a fantastic example of an uncontrolled river diversion. The FD2C model can also be used to monitor delta growth where direct field measurements are impossible or scarce.

Appendix A. Notation

$\breve{A}$	Fractional Velocity Increase in the downstream direction (m^{-1})
$\breve{B}$	Fractional Bed constriction in the downstream direction (m^{-1})
$\breve{D}$	Divergence in flow direction (m^{-1})
$\vec{\boldsymbol{d}}$	Unit vector aligned with flow direction (dimensionless)
Δl	distance downstream of the channel tip where the critical divergence point occurs; $\Delta l = x_{\breve{D}} - x_{\hat{\eta}}$ (m)
$\lvert\vec{U}\rvert$	Velocity magnitude (m/s)
$x_{\breve{D}}$	Critical divergence point along an axial channel transect (m)
$x_{\hat{\eta}}$	Elevation crest along an axial channel transect (m)
η	Bed elevation (m)

Author Contributions

J.B.S. conceived and led the study. J.D.E. did the first streakline mapping and analysis and proposed the criteria for $x_{\breve{D}}$. A.R.W. performed the 2016 bathymetric survey. K.M.S. contributed the statistical analyses of breakpoints. D.A.E. provided the numerical model simulations and Landsat imagery. J.B.S. wrote the manuscript with contributions from all co-authors. Kathryn Hurlbut performed the measurement of the numerical deltas.

© Author(s) 2018. CC BY 4.0 License.

7 Acknowledgements

Landsat imagery used in this study were downloaded from Google Earth Engine. Bathymetric maps of Wax Lake Delta are available in (Shaw, 2013; Shaw et al., 2016a). Imagery metadata, channel tip location estimates, and timeseries of area are all available in the supplementary material of this paper. This work was supported by a U.S. Department of Energy grant to J.B.S. (DESC0016163). Ashlyn Haynes contributed valuable work mapping many of the Landsat images for streaklines. Julie M. Cains illustrated Fig. 2.

References

Alpers, W. and Espedal, H. A.: Oils and surfactants, in Synthetic aperture radar marine user's manual, edited by C. R. Jackson and J. R. Appel, pp. 263–275, NOAA/NESDIS Office of Research and Applications. [online] Available from: http://www.webmail.sarusersmanual.com/ManualPDF/NOAASARManual_CH11_pg263-276.pdf (Accessed 21 January 2015), 2004.

Alpers, W., Campbell, G., Wensink, H. and Zhang, Q.: Underwater Topography, in Synthetic aperture radar marine user's manual, edited by C. R. Jackson and J. R. Appel, pp. 245–262, NOAA/NESDIS Office of Research and Applications. [online] Available from: http://www.webmail.sarusersmanual.com/ManualPDF/NOAASARManual_CH11_pg263-276.pdf (Accessed 21 January 2015), 2004.

Barras, J. A., Bernier, J. C., Morton, R. A. and (US), G. S.: Land Area Change in Coastal Louisiana, a Multidecadal Perspective (from 1956 to 2006), US Department of the Interior, US Geological Survey. [online] Available from: http://pubs.usgs.gov/sim/3019/ (Accessed 26 June 2012), 2008.

Cahoon, D. R., White, D. A. and Lynch, J. C.: Sediment infilling and wetland formation dynamics in an active crevasse splay of the Mississippi River delta, Geomorphology, 131(3–4), 57–68, doi:10.1016/j.geomorph.2010.12.002, 2011.

Caldwell, R. L. and Edmonds, D. A.: The effects of sediment properties on deltaic processes and morphologies: A numerical modeling study, J. Geophys. Res. - Earth Surf., 119, 961–982, doi:10.1002/2013JF002965, 2014.

Coffey, T. S. and Shaw, J. B.: Congruent Bifurcation Angles in River Delta and Tributary Channel Networks, Geophys. Res. Lett., 2017GL074873, doi:10.1002/2017GL074873, 2017.

Couvillion, B. R., Barras, J. A., Steyer, G. D., Sleavin, W., Fischer, M., Beck, H., Trahan, N., Griffin, B. and Heckman, D.: Land Area Change in Coastal Louisiana from 1932 to 2010, Scientific Investigations Map, Washington, D. C., 2011.

Edmonds, D. A. and Slingerland, R.: Mechanics of river mouth bar formation: Implications for the morphodynamics of delta distributary networks, J. Geophys. Res., 112(F02034), 14, doi:10.1029/2006JF000574, 2007.

Edmonds, D. A., Shaw, J. B. and Mohrig, D.: Topset-dominated deltas: A new model for river delta stratigraphy, Geology, 39(12), 1175–1178, doi:10.1130/G32358.1, 2011.

Erban, L. E., Gorelick, S. M. and Zebker, H. A.: Groundwater extraction, land subsidence, and sea-level rise in the Mekong Delta, Vietnam, Environ. Res. Lett., 9(8), 084010, doi:10.1088/1748-9326/9/8/084010, 2014.

© Author(s) 2018. CC BY 4.0 License.

Espedal, H. A., Johannessen, O. M. and Knulst, J.: Satellite detection of natural films on the ocean surface, Geophys. Res. Lett., 23(22), 3151–3154, doi:10.1029/96GL03009, 1996.

Esposito, C. R., Georgiou, I. Y. and Kolker, A. S.: Hydrodynamic and geomorphic controls on mouth bar evolution, Geophys. Res. Lett., 40(8), 1540–1545, doi:10.1002/grl.50333, 2013.

Fagherazzi, S., Edmonds, D. A., Nardin, W., Leonardi, N., Canestrelli, A., Falcini, F., Jerolmack, D., Mariotti, G., Rowland, J. C. and Slingerland, R. L.: Dynamics of River Mouth Deposits, Rev. Geophys., 2014RG000451, doi:10.1002/2014RG000451, 2015.

Galloway, W. E.: Process framework for describing the morphologic and stratigraphic evolution of deltaic depositional systems, edited by M. L. Broussard, Deltas Models Explor., 87–98, 1975.

Gao, J.: Bathymetric mapping by means of remote sensing: methods, accuracy and limitations, Prog. Phys. Geogr., 33(1), 103–116, doi:10.1177/0309133309105657, 2009.

Garabetian, F., Romano, J.-C., Paul, R. and Sigoillot, J.-C.: Organic matter composition and pollutant enrichment of sea surface microlayer inside and outside slicks, Mar. Environ. Res., 35(4), 323–339, doi:10.1016/0141-1136(93)90100-E, 1993.

Geleynse, N., Storms, J., Stive, M., Jagers, H. and Walstra, D.: Modeling of a mixed-load fluvio-deltaic system, Geophys Res Lett, 37(5), L05402, 2010.

Geleynse, N., Hiatt, M., Sangireddy, H. and Passalacqua, P.: Identifying environmental controls on the shoreline of a natural river delta, J. Geophys. Res. Earth Surf., 2014JF003408, doi:10.1002/2014JF003408, 2015.

Hiatt, M. and Passalacqua, P.: Hydrological connectivity in river deltas: The first-order importance of channel-island exchange, Water Resour. Res., 51(4), 2264–2282, doi:10.1002/2014WR016149, 2015.

Hiatt, M. and Passalacqua, P.: What Controls the Transition from Confined to Unconfined Flow? Analysis of Hydraulics in a Coastal River Delta, J. Hydraul. Eng., 143(6), 03117003, doi:10.1061/(ASCE)HY.1943-7900.0001309, 2017.

Holm, G. O. and Sasser, C. E.: Differential salinity response between two Mississippi River subdeltas: implications for changes in plant composition, Estuaries Coasts, 24(1), 78–89, 2001.

Hühnerfuss, H., Gericke, A., Alpers, W., Theis, R., Wismann, V. and Lange, P. A.: Classification of sea slicks by multifrequency radar techniques: New chemical insights and their geophysical implications, J. Geophys. Res. Oceans, 99(C5), 9835–9845, doi:10.1029/93JC03308, 1994.

Jiménez-Robles, A. M., Ortega-Sánchez, M. and Losada, M. A.: Effects of basin bottom slope on jet hydrodynamics and river mouth bar formation, J. Geophys. Res. Earth Surf., 121(6), 2016JF003871, doi:10.1002/2016JF003871, 2016.

Johnson, W., Sasser, C. and Gosselink, J.: Succession of vegetation in an evolving river delta, Atchafalaya Bay, Louisiana, J. Ecol., 973–986, 1985.

Kundu, P. K., Cohen, I. M. and Dowling, D.: Fluid Mechanics, Fifth Edition, 5 edition., Academic Press, Waltham, MA., 2011.

Leonardi, N., Canestrelli, A., Sun, T. and Fagherazzi, S.: Effect of tides on mouth bar morphology and hydrodynamics, J. Geophys. Res. Oceans, 118(9), 4169–4183, doi:10.1002/jgrc.20302, 2013.

© Author(s) 2018. CC BY 4.0 License.

Li, C., Roberts, H., Stone, G. W., Weeks, E. and Luo, Y.: Wind surge and saltwater intrusion in Atchafalaya Bay during onshore winds prior to cold front passage, Hydrobiologia, 658(1), 27–39, doi:10.1007/s10750-010-0467-5, 2011.

Li, X. and Damen, M. C. J.: Coastline change detection with satellite remote sensing for environmental management of the Pearl River Estuary, China, J. Mar. Syst., 82, S54–S61, doi:10.1016/j.jmarsys.2010.02.005, 2010.

Liang, M., Van Dyk, C. and Passalacqua, P.: Quantifying the Patterns and Dynamics of River Deltas Under Conditions of Steady Forcing and Relative Sea-Level Rise, J. Geophys. Res. Earth Surf., 2015JF003653, doi:10.1002/2015JF003653, 2016.

Nardin, W. and Fagherazzi, S.: The effect of wind waves on the development of river mouth bars, Geophys. Res. Lett., 39(12), n/a–n/a, doi:10.1029/2012GL051788, 2012.

NOAA: Saint Clair River, [online] Available from: http://www.charts.noaa.gov/PDFs/14852.pdf (Accessed 5 July 2017), 2017.

Olliver, E. A. and Edmonds, D. A.: Defining the ecogeomorphic succession of land building for freshwater, intertidal wetlands in Wax Lake Delta, Louisiana, Estuar. Coast. Shelf Sci., doi:10.1016/j.ecss.2017.06.009, 2017.

Özsoy, E. and Ünlüata, Ü.: Ebb-tidal flow characteristics near inlets, Estuar. Coast. Shelf Sci., 14(3), doi:10.1016/S0302-3524(82)80015-7, 1982.

Peyronnin, N. S., Caffey, R. H., Cowan, J. H., Justic, D., Kolker, A. S., Laska, S. B., McCorquodale, A., Melancon, E., Nyman, J. A., Twilley, R. R., Visser, J. M., White, J. R. and Wilkins, J. G.: Optimizing Sediment Diversion Operations: Working Group Recommendations for Integrating Complex Ecological and Social Landscape Interactions, Water, 9(6), 368, doi:10.3390/w9060368, 2017.

Rahman, A. F., Dragoni, D. and El-Masri, B.: Response of the Sundarbans coastline to sea level rise and decreased sediment flow: A remote sensing assessment, Remote Sens. Environ., 115(12), 3121–3128, doi:10.1016/j.rse.2011.06.019, 2011.

Rangoonwala, A., Jones, C. E. and Ramsey, E.: Wetland shoreline recession in the Mississippi River Delta from petroleum oiling and cyclonic storms, Geophys. Res. Lett., 43(22), 2016GL070624, doi:10.1002/2016GL070624, 2016.

Romeiser, R. and Alpers, W.: An improved composite surface model for the radar backscattering cross section of the ocean surface: 2. Model response to surface roughness variations and the radar imaging of underwater bottom topography, J. Geophys. Res. Oceans, 102(C11), 25251–25267, doi:10.1029/97JC00191, 1997.

Shaw, J. B. and Mohrig, D.: The importance of erosion in distributary channel network growth, Wax Lake Delta, Louisiana, USA, Geology, 42(1), 31–34, doi:10.1130/G34751.1, 2014.

Shaw, J. B., Ayoub, F., Jones, C. E., Lamb, M. P., Holt, B., Wayne Wagner, R., Coffey, T., Austin Chadwick, J. and Mohrig, D.: Airborne Radar Imaging of Subaqueous Channel Evolution in Wax Lake Delta, Louisiana, USA, Geophys. Res. Lett., 2016GL068770, doi:10.1002/2016GL068770, 2016a.

Shaw, J. B., Mohrig, D. and Wagner, R. W.: Flow patterns and morphology of a prograding river delta, J. Geophys. Res. Earth Surf., 2015JF003570, doi:10.1002/2015JF003570, 2016b.

Shaw, J. B., Miller, K. and McElroy, B.: Island Formation Resulting from Radially Symmetric Flow Expansion, J. Geophys. Res. Earth Surf., 2017JF004464, doi:10.1002/2017JF004464, 2018.

© Author(s) 2018. CC BY 4.0 License.

Wilson, C., Goodbred, S., Small, C., Gilligan, J., Sams, S., Mallick, B. and Hale, R.: Widespread infilling of tidal channels and navigable waterways in human-modified tidal deltaplain of southwest Bangladesh, Elem Sci Anth, 5(0), doi:10.1525/elementa.263, 2017.

Wright, L.: Sediment transport and deposition at river mouths: a synthesis, Bull. Geol. Soc. Am., 88(6), 857–868, 1977.

Wu, X., Bi, N., Xu, J., Nittrouer, J. A., Yang, Z., Saito, Y. and Wang, H.: Stepwise morphological evolution of the active Yellow River (Huanghe) delta lobe (1976–2013): Dominant roles of riverine discharge and sediment grain size, Geomorphology, 292, 115–127, doi:10.1016/j.geomorph.2017.04.042, 2017.

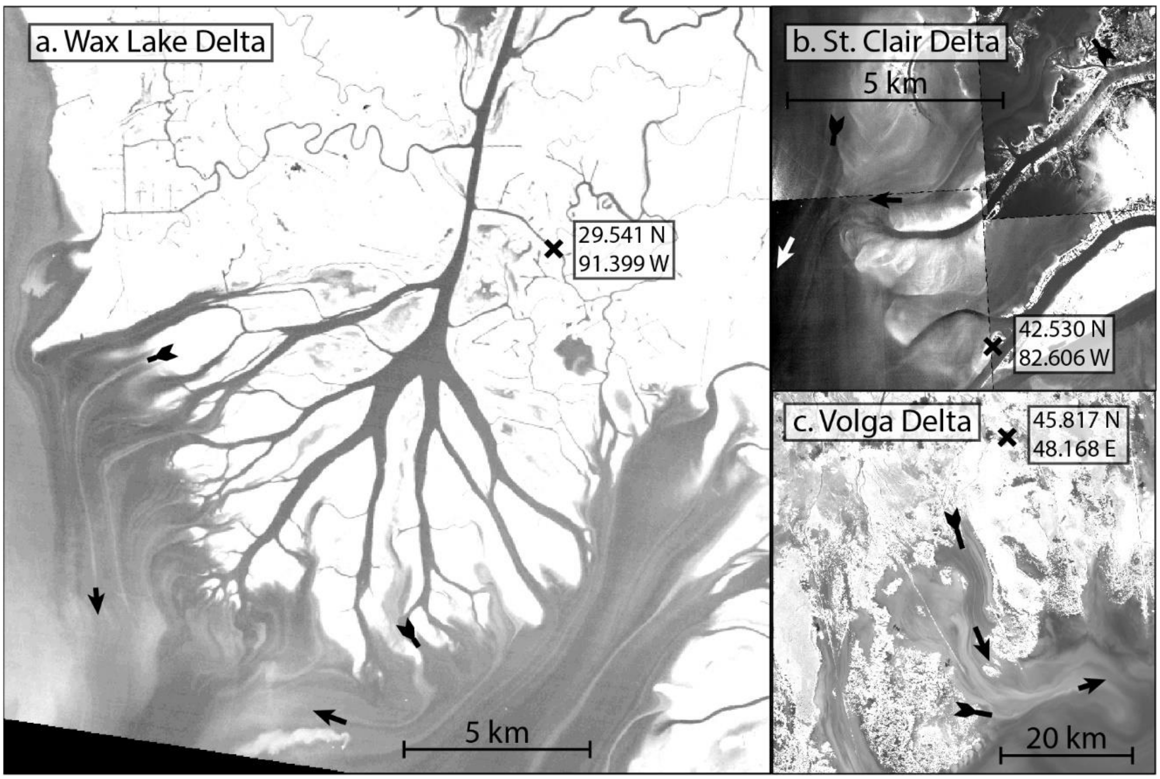

Figure 1: Images of river deltas exhibiting streaklines. Arrows trace some of the streaklines. (a) Wax Lake Delta (Landsat image LT50230402011002CHM01 Band 4). (b) the Saint Clair Delta in Michigan, USA (Digital Orthophoto Quads Saint Clair Flats NE, NW, SW, SE, IR band). (c) Portion of the Volga Delta in Russia (Landsat LC08_L1TP_168028_20170501_01 Band 4).

© Author(s) 2018. CC BY 4.0 License.

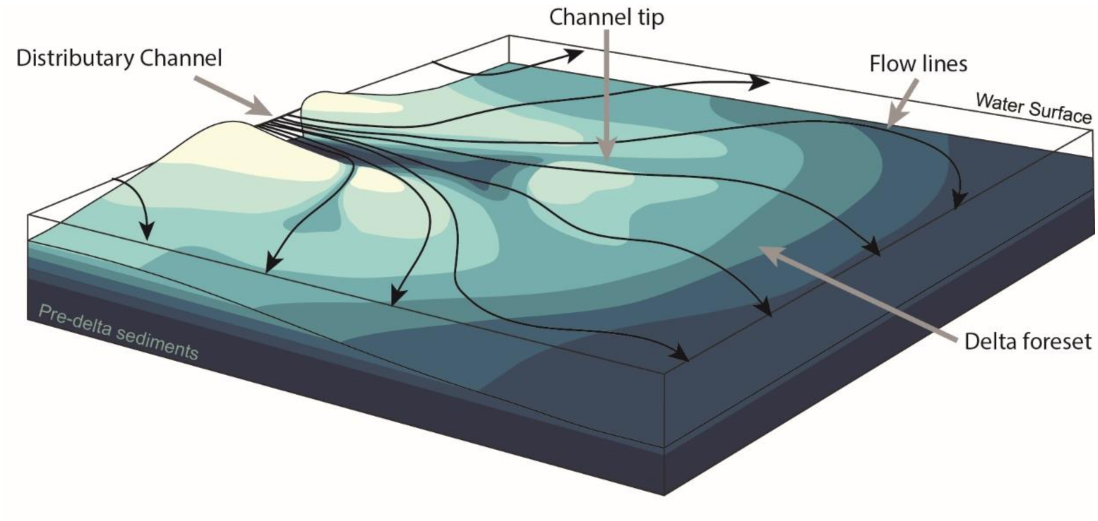

Figure 2: Schematic diagram of delta front morphology and streakline behavior. The colormap shows a distributary channel tip on a delta front with dark colors representing deep areas and light colors representing shallow areas. Streaklines are shown as black solid lines. The FD2B method takes advantage of lateral flow direction divergence through the shoaling reach of the channel and lateral flow direction convergence on the delta front. Hence, the end of shoaling and channel tips occur roughly where.

© Author(s) 2018. CC BY 4.0 License.

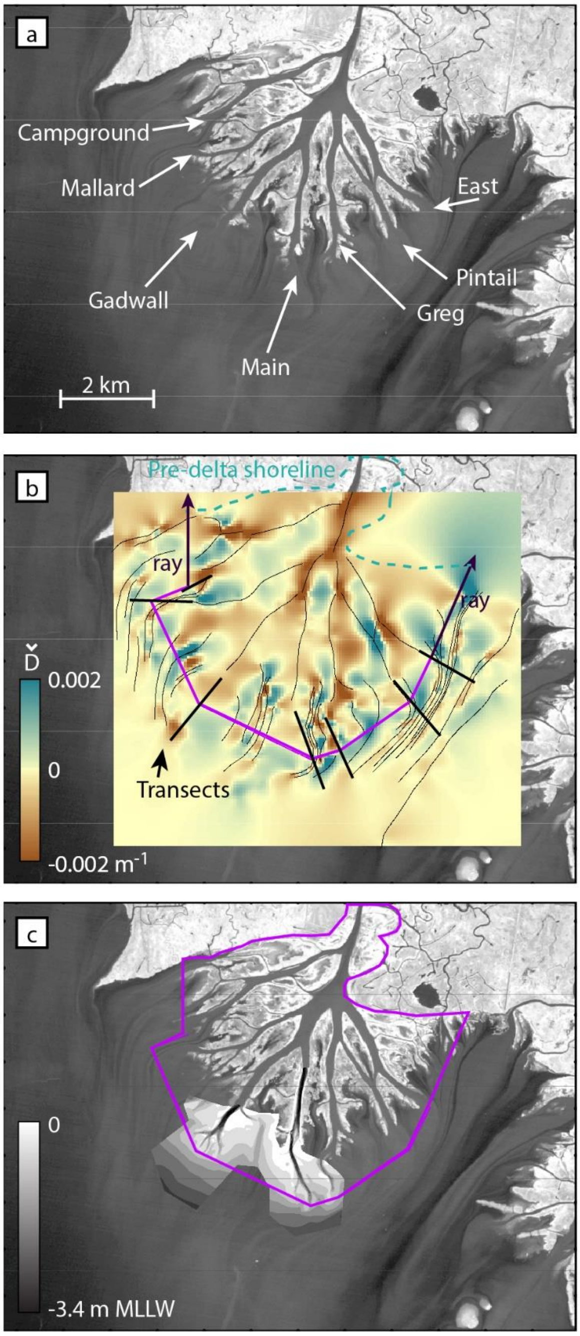

Figure 3. Method for converting imagery into channel tips and delta area. (a) Landsat image displaying streaklines (14 October 2010; Supplementary Material). The seven primary distributary channels are labelled. (b) Streaklines (thin black lines) are mapped manually on the delta front, and lines are also placed down the center of subaerially emergent distributary channels. The $\check{D}$ field is interpolated from these strealklines (colormap). Thick black lines are transects extending from the seven primary distributary channels. The estimated location $x_{\hat{\eta}}$ along each transect is connected via the purple line and rays connect channel tips to the pre-delta shoreline to close the area. (c) The interpreted area of the submerged delta is shown. A bathymetric map from June 2010 referenced to mean lower low water (MLLW) shows how the interpreted channel tips compare to direct measurements.

© Author(s) 2018. CC BY 4.0 License.

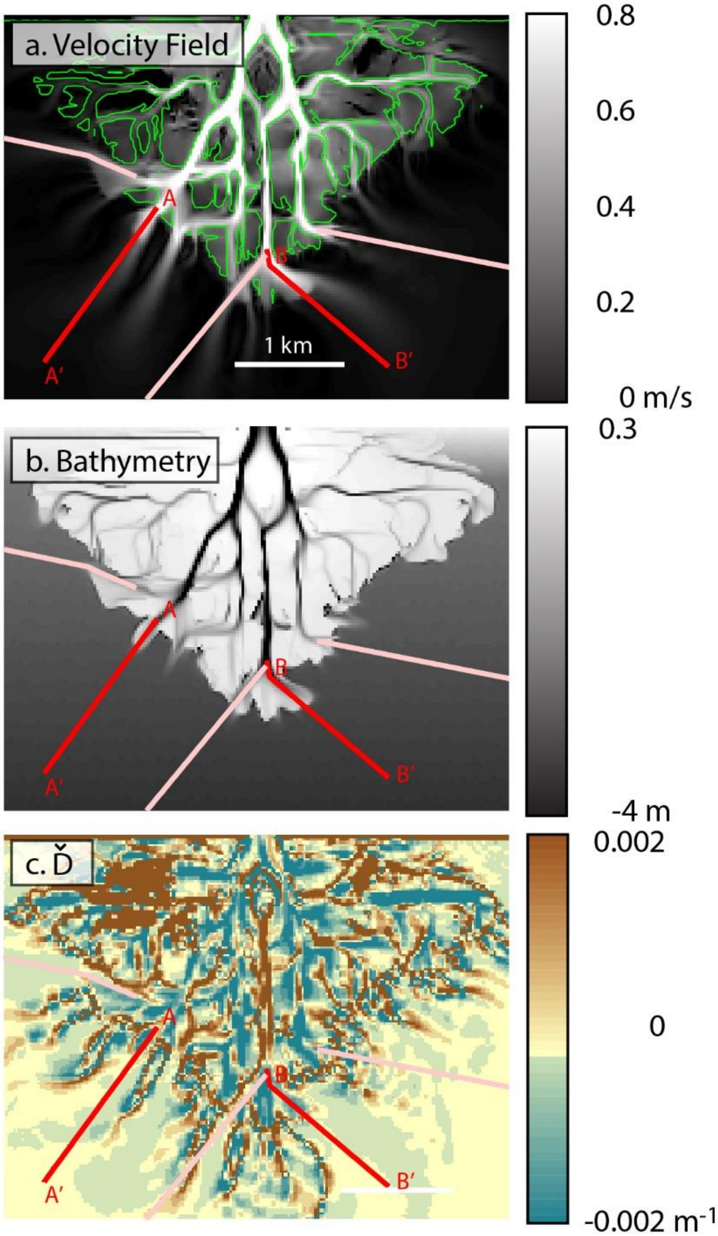

Figure 4. Method for comparing $\check{D}$ to bathymetry in numerical delta simulations. (a) The velocity field and -0.3 m MSL (green) contour are displayed and transects (pink and red lines) are drawn extending from the largest distributary network channels. (b) The bathymetric profile is collected along each transect. (c) $\check{D}$ is calculated, and transects of $\check{D}$ are collected along the transects. Transects A-A' and B-B' are shown in Figure 5.

© Author(s) 2018. CC BY 4.0 License.

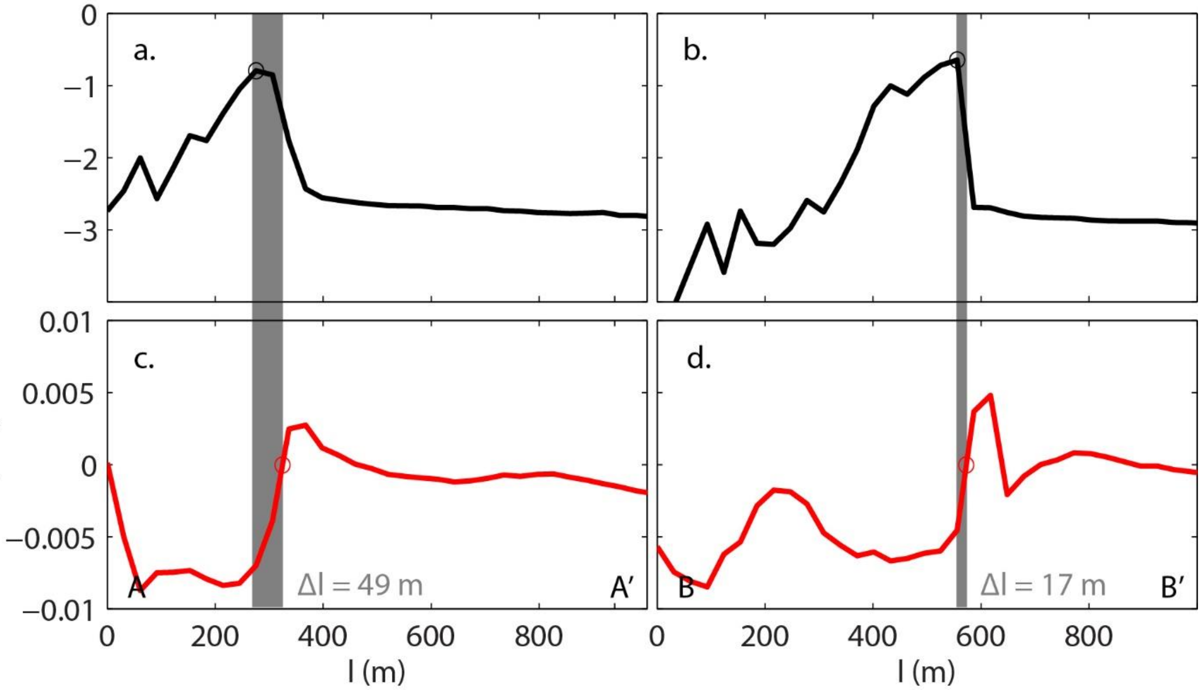

Figure 5. Comparison of bathymetry (η; plots a and b) and divergence of flow direction (Ď; plots c and d) for transects A-A' (plots a, c) and B-B' (plots b, d). Δl is the location where Ď changes from positive to negative (red circle) minus the bathymetric maximum of the channel tip (black circle). The distribution of Δl is shown in Figure 6.

© Author(s) 2018. CC BY 4.0 License.

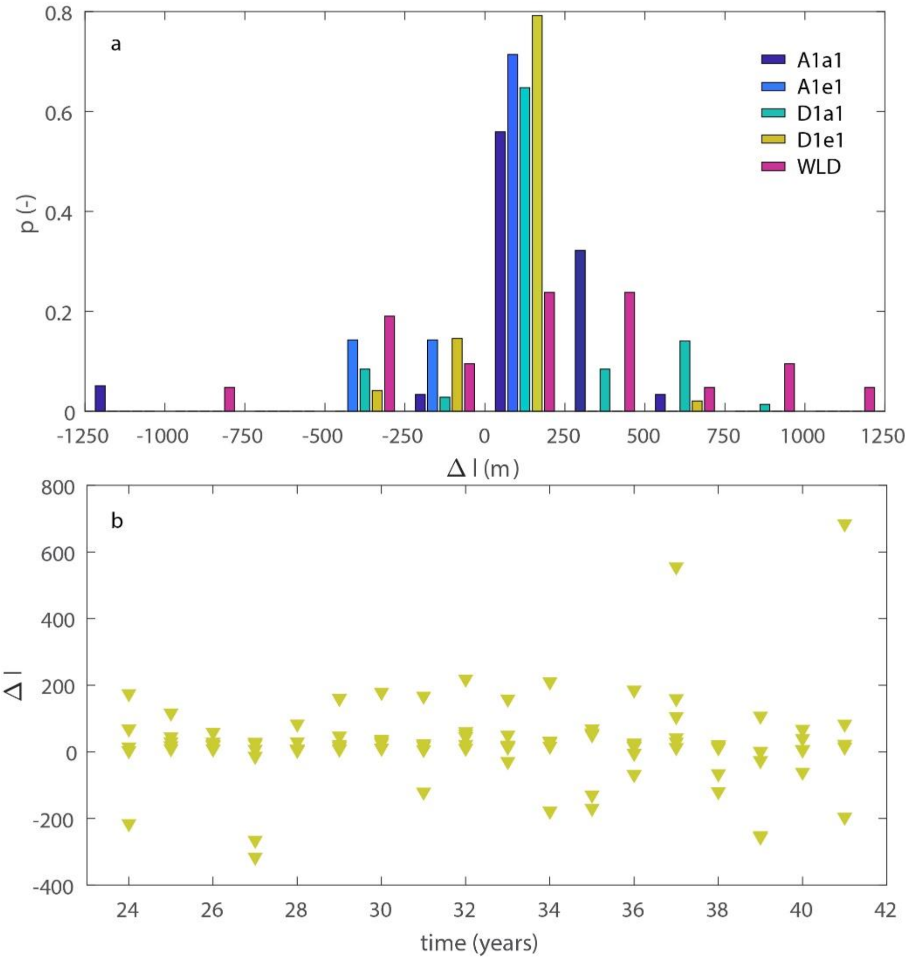

Figure 6. (a) Normalized histogram of Δl for numerical model A1a1 (dark blue), A1e1 (light blue), D1a1 (seafoam) and D1e1 (orange) compared with measurements from the Wax Lake Delta (yellow). All histograms are binned at 250 m intervals. Descriptive statistics of these populations are shown in Table 2. (b) The location of Δl as a function of time (model years) for delta run 'D1e1.' There is no significant trend in the location of Δl over time.

© Author(s) 2018. CC BY 4.0 License.

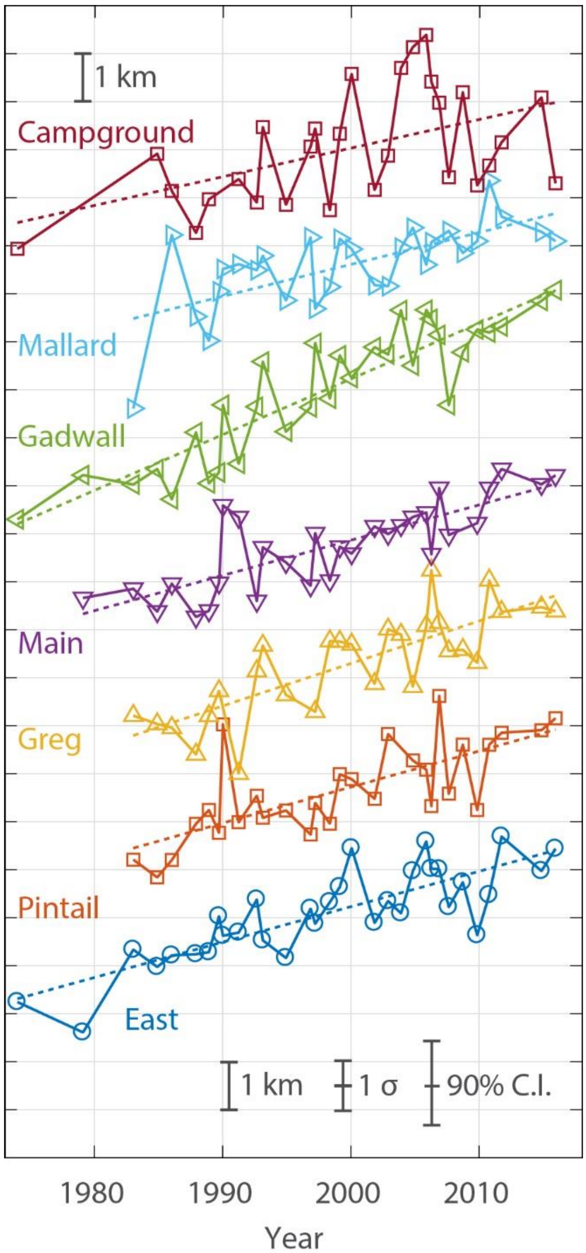

Figure 7. Growth of individual channels over time. Each series is plotted at the same scale (horizontal lines = 1 km, vertical lines 10 years), but are shifted vertically for clarity. The uncertainty associated with Δl measured at Wax Lake Delta (Figure 6a) is shown with a standard deviation (σ) and 90% confidence interval (C.I.) at the bottom. The primary distributary channels are shown from West to East: Campground Pass (maroon squares), Mallard Pass (turquoise right-pointing triangles), Gadwall Pass (green left-pointing triangles), Main Pass (purple down-pointing triangles), Greg Pass (yellow up-pointing triangles), Pintail Pass (red squares), and East Pass (blue circles). Dashed lines show linear regressions of each dataset. East Pass's regression includes a statistically significant break-point (see section 4) in February 1983.

© Author(s) 2018. CC BY 4.0 License.

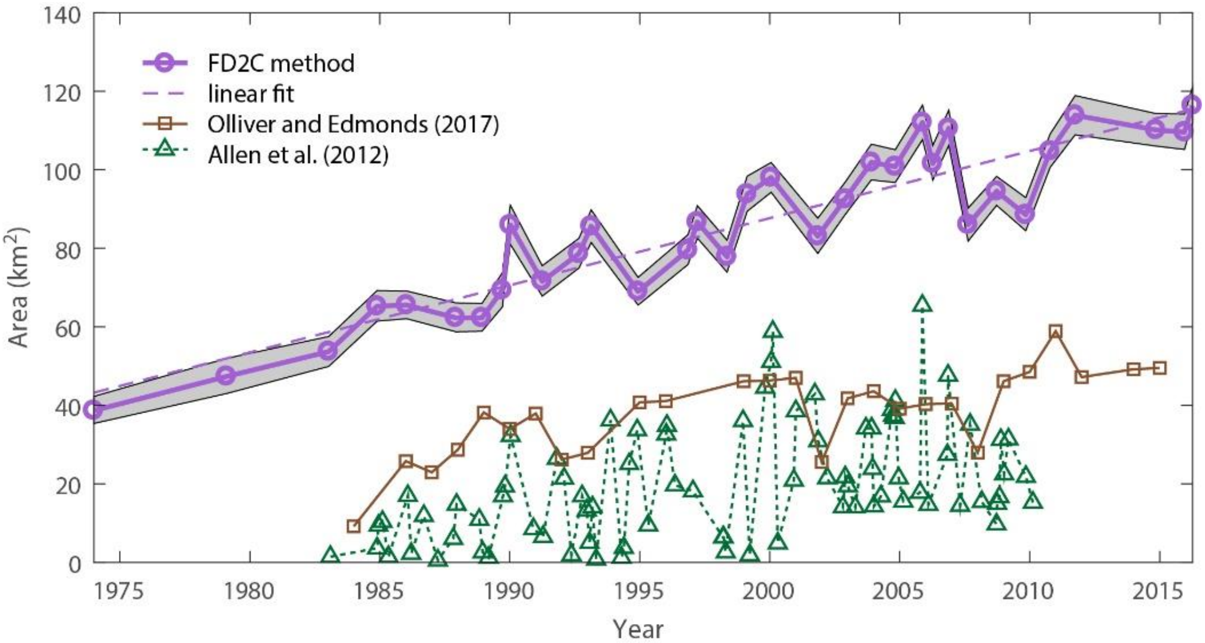

Figure 8. Area of the Wax Lake Delta as a function of time. Purple circles show the growth of the subaqueous Wax Lake Delta using the FD2C method. The gray region shows the 1σ deviation (16th to 84th percentile) of area found from Monte Carlo sampling of Δl (Section 4). The dashed line shows the linear fit, with a growth rate of 1.83 ± 0.14 km2/yr. Brown squares and greed triangles show the subaerial growth as documented by Olliver and Edmonds (2017) and Allen et al. (2012).

	WLD	A1a1	A1e1	D1a1	D1e1
Mean	145	140	-44	142	185
Median	132	196	12	52	76
Std	522	434	182	273	284
Iqr	701	233	156	171	254
Skew	0.09	-3.59	-1.45	0.77	1.98
Min	-952	-1849	-499	-398	-316
Max	1300	521	156	965	1794
n (number measurements)	21	79	14	98	185
n misses	0	20	0	27	0

Table 1. Statistic describing the distribution of Δ*l* for the Wax Lake Delta (WLD) and four delta simulations.